



RESEARCH ARTICLE

In vivo analysis of vascularization and biocompatibility of electrospun polycaprolactone fibre mats in the rat femur chamber

Sarah Gniesmer^{1,2} | Ralph Brehm³ | Andrea Hoffmann^{2,4} | Dominik de Cassan⁵ | Henning Menzel⁵ | Anna-Lena Hoheisel^{2,6} | Birgit Glasmacher^{2,6} | Elmar Willbold^{2,7}  | Janin Reifenrath^{2,7} | Mathias Wellmann⁷ | Nils Ludwig⁸ | Frank Tavassol¹ | Ruediger Zimmerer¹ | Nils-Claudius Gellrich¹ | Andreas Kampmann^{1,2} 

¹Department of Oral and Maxillofacial Surgery, Hannover Medical School, Hannover, Germany

²NIFE—Lower Saxony Centre for Biomedical Engineering, Implant Research and Development, Hannover, Germany

³Institute for Anatomy, University of Veterinary Medicine Hannover, Hannover, Germany

⁴Department of Orthopedic Surgery, Laboratory for Biomechanics and Biomaterials, Graded Implants and Regenerative Strategies, Hannover Medical School, Hannover, Germany

⁵Institute for Technical Chemistry, University of Technology, Braunschweig, Germany

⁶Institute for Multiphase Processes, Leibniz University of Hannover, Hannover, Germany

⁷Department of Orthopedic Surgery, Hannover Medical School, Hannover, Germany

⁸Department of Pathology, University of Pittsburgh School of Medicine, Pittsburgh, PA

Correspondence

Andreas Kampmann, Department of Oral and Maxillofacial Surgery, Hannover Medical School, Carl-Neuberg-Str. 1, Hannover 30625, Germany.

Email: kampmann.andreas@mh-hannover.de

Funding information

DFG FOR 2180, Grant/Award Number: KA 4236/1-1

Abstract

In orthopaedic medicine, connective tissues are often affected by traumatic or degenerative injuries, and surgical intervention is required. Rotator cuff tears are a common cause of shoulder pain and disability among adults. The development of graft materials for bridging the gap between tendon and bone after chronic rotator cuff tears is essentially required. The limiting factor for the clinical success of a tissue engineering construct is a fast and complete vascularization of the construct. Otherwise, immigrating cells are not able to survive for a longer period of time, resulting in the failure of the graft material. The femur chamber allows the observation of microhaemodynamic parameters inside implants located in close vicinity to the femur in repeated measurements in vivo. We compared a porous polymer patch (a commercially available porous polyurethane-based scaffold from Biomerix™) with electrospun polycaprolactone (PCL) fibre mats and chitosan (CS)-graft-PCL modified electrospun PCL (CS-g-PCL) fibre mats in vivo. By means of intravital fluorescence microscopy, microhaemodynamic parameters were analysed repetitively over 20 days at intervals of 3 to 4 days. CS-g-PCL modified fibre mats showed a significantly increased vascularization at Day 10 compared with Day 6 and at Day 14 compared with the porous polymer patch and the unmodified PCL fibre mats at the same day. These results could be verified by histology. In conclusion, a clear improvement in terms of vascularization and biocompatibility is achieved by graft-copolymer modification compared with the unmodified material.

KEYWORDS

angiogenesis, biocompatibility, electrospinning, intravital microscopy, microhaemodynamics, PCL fibre mats

This is an open access article under the terms of the Creative Commons Attribution-NonCommercial License, which permits use, distribution and reproduction in any medium, provided the original work is properly cited and is not used for commercial purposes.

© 2019 The Authors Journal of Tissue Engineering and Regenerative Medicine Published by John Wiley & Sons Ltd

1 | INTRODUCTION

In orthopaedic medicine, connective tissues are often affected by traumatic or degenerative injuries, and surgical intervention is required. Rotator cuff tears are a common cause of shoulder pain and disability among adults. The aetiopathogenesis of rotator cuff tears is not resolved finally. Several theories concerning the reasons of rotator cuff tears distinguishing between extrinsic and intrinsic factors were discussed in Gai Via, De Cupis, Spoliti, and Oliva (2013). In addition to the unknown aetiopathogenesis of rotator cuff tears, the healing process in tendon-to-bone interfaces is very slow because of low vascularization in tendon tissue. Thereby, the nutrition and the removal of inflammatory products are impeded. At the present time, several strategies for the management of rotator cuff injuries are discussed, but numerous attempts to rebuild the transition zone and to restore a functional enthesis have been shown to be unsuccessful (Boileau et al., 2005; Jost, Zumstein, Pfirrmann, & Gerber, 2006). The structure of the transition zone between tendon and bone, called enthesis, is mechanically and biologically complex. The importance of this structure arises from its function. The attachment of two dissimilar materials results in stress singularities at their interface. The transitional tissue of the enthesis that shows structural and compositional gradients reduces stress concentrations and warrants an optimal transmission of forces between the stiff, brittle bone, and the tough, extensible tendon (Zelzer, Blitz, Killian, & Thomopoulos, 2014; Lu & Thomopoulos, 2013). The fibrocartilaginous enthesis in the rotator cuff is classified in four distinct zones of tissue with a structurally continuous gradient from uncalcified tendon to uncalcified fibrocartilage to calcified fibrocartilage to calcified bone. The junctions between distinct tissue types are prone to injury, and unfortunately, their recovery following surgical repair is only poor. Injuries are more frequent in fibrocartilaginous enthesis than in fibrous insertions (Apostolakis et al., 2014).

During the early healing process, the tendon-to-bone junction is not resilient, because the complex tendon-to-bone-construct is replaced by fibrotic tissue. After months and weeks, the biomechanical strength increases due to the remodelling process at the tendon-to-bone junction (Gulotta, Kovacevic, Packer, Deng, & Rodeo, 2011). However, the healing process results solely in a repair of the damaged junction, thus leading to the formation of scar tissue and not in the regeneration of the naturally occurring tendon-to-bone interface with its organized distinct composition of four zones (Rodeo, 2007).

In case of a chronic rotator cuff tear, the typically long latency between occurrence, diagnosis, and treatment leads to chronic changes in the musculotendinous unit. Muscle atrophy and fatty infiltrations of the muscle arise through the loss of muscle activity and the loss of pretension (Gerber, Meyer, Schneeberger, Hoppeler, & Von Rechenberg, 2004; Gerber et al., 2009). Consecutively, the tendon retracts, and surgical repair is complicated (Meyer, Wieser, Farshad, & Gerber, 2012). To accomplish surgical tendon repair, the gap between bone and tendon must be bridged by applying tension to extend the tendon, or the gap has to be closed by augmentation with a graft (Meyer, Gerber, von Rechenberg, Wirth, & Farshad, 2011). All

implantations lead to an inflammatory response either because of the surgical trauma or as a reaction to the implant itself. The inflammatory response is based on the well-known foreign body reaction depending on the material and its surface characteristics. To reduce this reaction, implants can be modified with coatings or used as carriers for medication and growth factors (Ferracini et al., 2018). The used materials must be biocompatible to prevent adverse immunological reaction. Additionally, the structure of implants is of great importance for cells to attach, proliferate, and migrate. The survival of the implant and thus the success of the therapy after implant placement are dependent on the migration of the cells and their supply with oxygen and nutrients as well as the removal of waste (Lovett, Lee, Edwards, & Kaplan, 2009). Therefore, the key factor is adequate angiogenesis, especially in the early stages after implantation. Previous *in vivo* investigations of angiogenic processes after the application of implants were carried out mostly in soft tissue models, such as the dorsal skinfold chamber (Rücker et al., 2006). Recently, different hard tissue models like the cranial window have been described (Sinikovic et al., 2011). With respect to orthopaedic applications, the examination of implants in the area of long tubular bones is more appropriate. The femur chamber model in mice allows the assessment of the microcirculation in a femoral defect model in immediate vicinity of the bone (Tavassol et al., 2011). In this study, we adapted this model to allow the application in rats without a bone defect. Therewith, information about angiogenesis can be given in the target area of orthopaedic implants.

Implants, which are not intended to remain permanently in the body and difficult to remove after healing, should be biodegradable without toxic remains. The rate of degradation should correspond to the rate of tissue restoration. The physiological situation at the defect site should be restored by invading cells in the long term whereas the implant is transformed into harmless degradation products that can be metabolized.

In line with these arguments, polycaprolactone (PCL) is used in various biomedical applications because of its biocompatibility, adequate mechanical properties, and slow degradation *in vivo* (Lam, Hutmacher, Schantz, Woodruff, & Teoh, 2008; Dash & Konkimalla, 2012). PCL can be processed by electrospinning, which allows a controlled design of fibre alignment, porosity, fibre diameter, and pore size (Font Tellado, Balmayor, & Griensven, 2015). Although PCL is biocompatible, its surface is hydrophobic and thus not particularly attractive for cell attachment and growth (Venugopal, Ma, Yong, & Ramakrishna, 2005). Therefore, PCL is unattractive for biomedical applications (Nair & Laurencin, 2007). Furthermore, because PCL is an aliphatic polyester, it lacks access to easy modifications, and chemically more reactive moieties have to be introduced by various approaches such as plasma or wet chemical treatment, blending, and attachment of graft copolymers (Fu, Sammons, Bertóti, Jenkins, & Dong, 2011; Tallawi et al., 2015; de Cassan et al., 2018). These modifications can help overcome these weaknesses of PCL, while maintaining good properties, and create implants applicable in a variety of orthopaedic areas, for example, the use in therapy of chronic rotator cuff tears.

Therefore, the purpose of this study is to characterize the vascularization and biocompatibility of PCL-based implants in the hard tissue model of femur chamber in rats, in comparison with commercially available implant material.

2 | MATERIALS AND METHODS

2.1 | Implants

For the experimental groups, electrospun fibre mats were produced by electrospinning of poly- ϵ -caprolactone ($M_n = 80,000$, Sigma-Aldrich Chemie GmbH, Taufkirchen, Germany; PCL) and trifluoroethanol (abcr GmbH, Karlsruhe, Germany). A PCL solution of 170 mg/ml in trifluoroethanol was loaded into a 10-ml syringe (B. Braun, Melsungen, Germany) connected by polyethylene tubing to an electrospinning emitter (B. Braun Needle 8 G, blunt tip, Melsungen, Germany). A rotating steel drum covered with aluminium foil served as a collector. The scaffolds were produced with 2 m/s for unorientated fibres. The voltage was set to 25 kV and the emitter to collector distance to 25 cm. The fibre mat thickness of 300 μm arose from the solution flow rate of 4 ml/hr.

As a second experimental group, the same PCL fibre mats were additionally modified with chitosan, called chitosan-g-PCL. For synthesis, chitosan-PCL graft copolymers were crystallized on PCL nanofibres, as described recently (de Cassan et al., 2018). Thereby, chitosan is presented at the surface of the fibre.

As a control group, a commercially available porous polymer scaffold (Biomerix RCR Patch, Biomerix Corporation, Somerset, USA; purchased from Cellon, Bascharage, Luxembourg; Encalada-Diaz et al., 2011) was used. This biocompatible scaffold has an interconnected 3D network of pores with a pore size of 100 to 250 μm . The material is designed to mimic the nature and function of the extracellular matrix for regenerative medicine research (Encalada-Diaz et al., 2011). For further characterization, scaffolds of each group were stamped with a circular cutter to a diameter of 15 (mass analysis) and 25 mm (porosity). In the case of fibre mats, material for the implants as well as for the further characterization is obtained from the middle area. In this area, the structure of the fibre mats is more homogeneous than in the peripheral areas.

For in vivo experiments, scaffolds of each group were cut into pieces of 3 \times 5 mm and shrink-wrapped in sterilization pouches (SteriClin, Vereinigte Papierwarenfabriken, Feuchtwangen, Germany). The sterilization was performed by beta radiation with a dose of 25 kGy (using a Rhodotron TT 100 e-beam accelerator, Mediscan, Kremsmünster, Austria).

2.2 | Evaluation of porosity and pore diameter

The porosity of the fibrous scaffolds was determined by the gravimetric method. This method uses the mass, density, and dimensions of a sample to calculate the porosity (equation below).

$$\Phi = \frac{V_E}{V_T} = 1 - \frac{4 \cdot m}{\rho \cdot s \cdot \pi \cdot d^2},$$

with porosity Φ , empty volume V_E in cm^3 , total volume V_T in cm^3 , mass m in g, polymeric density ρ in g/cm^3 , sample thickness s in cm, and sample diameter d in cm.

The sample mass was determined with a high-precision scale. For determination of the thickness, the sample was cut in half in liquid nitrogen with a razor blade. Images of the cutting edge were taken with a scanning electron microscope (SEM, Hitachi S-3400) and analysed with an image analysis software (AxioVision, Carl Zeiss).

The pore diameter was determined with a capillary flow porometer (3 Gzh, Quantachrome GmbH & Co.KG). Porofil® (Quantachrome GmbH & Co.KG) was used as wetting liquid to spontaneous fill all pores in the sample. The solid-gas interface was thereby replaced by a solid-liquid interface. Pressure from a non-reactant gas was gradually increased on the top side of the sample. When the energy of the non-reactant gas exceeds the interfacial free energy of the solid/liquid interface, Porofil® was replaced by the non-reactant gas. Gas flow occurs through the largest pore of the sample (Jena & Gupta, 2001). Further pressure increase emptied smaller pores.

The software 3Gwin (Quantachrome GmbH & Co.KG) detected the flow rate over the pressure. A wet (liquid-filled) curve and a dry (liquid-free) curve were measured for each sample. From the collected data, the pore diameter was calculated by the software using following equation:

$$D = \frac{4 \gamma \cos \theta}{p}$$

Where D is the pore diameter, γ the surface tension of the wetting liquid, θ the contact angle of the wetting liquid, and p the differential pressure (Li, Frey, & Joo, 2006).

2.3 | Experimental protocol

Twenty-six Lewis/Han Ztm rats were equipped with femur chambers. Scaffolds consisting of either a porous polymer patch (control; $n = 8$) or unmodified PCL fibre mats (PCL; $n = 9$) or chitosan (CS)-graft-PCL modified electrospun PCL fibre mats (CS-g-PCL; $n = 9$) were implanted. Intravital fluorescence microscopy (IVM) analysis of volumetric blood flow, wall shear rate, leukocyte-endothelial cell interaction, macromolecular leakage, and functional capillary density were performed immediately as well as 3, 6, 10, 14, 17, and 20 days after implantation.

2.4 | Animals

All experiments were conducted in accordance with the German legislation for the protection of animals and the Guide for the Care and Use of Laboratory Animals (8th edition, 2011). The experiments were approved by the competent authority (Niedersächsisches Landesamt für Verbraucherschutz und Lebensmittelsicherheit, reference number 33.12-42502-04-15/2015). Male Lewis rats with a body weight of

383 ± 65 g were used for the study with an age of 27 ± 12 weeks. All animals were housed individually per cage at room temperature between 22°C and 24°C and a relative humidity of 60–65% with a 12-hr day-night cycle. The rats had free access to tap water and standard pellet food (1328 Hybridpellet, Altromin, Lage/Westphalia, Germany) at all times.

2.5 | Anaesthesia

The preparation of the femur chamber and repeated IVM was executed under inhalational anaesthesia (EZ-7000 Classic System, PLEXX, Elst/The Netherlands) by isoflurane. The animals were placed in an induction chamber, and anaesthesia was induced with 5% isoflurane (isoflurane, Isofluran CP®, 1 ml/ml, cp pharma, Burgdorf, Germany) until loss of righting reflex. The anaesthesia depth was determined with the aid of the toe pinch. After induction, the animals were placed in lateral position on a heating mat to protect the animals against hypothermia. Animals remained anaesthetized with the aid of a nose cone with 2–3% isoflurane in oxygen.

2.6 | Preparation of the rat femur chamber

The animals received a pain medication including butorphanol (butorphanol, 0.05 mg/kg, Torbugesic 10 mg/ml, cp pharma, Burgdorf, Germany) and carprofen (carprofen, 5 mg/kg, Carprosol 50 mg/ml, cp pharma, Burgdorf, Germany) preoperatively. After shaving, depilating and disinfection of the left hind limb, the skin was cut over the length of the femur, and the musculature in this field was carefully separated to expose the femur. As local anaesthesia lidocaine (lidocaine, 5 mg/kg, Lidocainhydrochlorid 2%, bela-pharm, Vechta, Germany) was applied directly on the femur before fixation of the chamber frame (see Figure 1 for details of the chamber design) and the trochanter major was removed using a dental burr (Komet dental, Gebr. Brasseler GmbH & Co. KG, Lemgo, Germany). Suture material (4-0, Vicryl™Plus, braided, absorbable, Johnson & Johnson Medical GmbH, Ethicon Deutschland,

Norderstedt, Germany) was placed around the femur for later fixation of the implant to the bone. The femur chamber (Figure 1) was attached with two bone screws (MF-corticalis screws, 1.3 × 4 mm, DePuy Synthes, Johnson & Johnson Medical GmbH, Umkirch, Germany) dorsal and distal of the observation window. After filling the chamber with physiological saline solution (NaCl 0.9%, B. Braun, Melsungen, Germany), the chamber was closed with a cover glass (Ø10 mm, Thermo Scientific, Braunschweig, Germany), which was fixed with a circlip (Central Research Devices Service Unit, Hannover Medical School, Hannover, Germany). The skin was adapted to the femur chamber (5-0 Ethilon*II, Polyamide, monofil, nonresorbable, Johnson & Johnson Medical GmbH, Ethicon Deutschland, Norderstedt, Germany) and sutured (4-0, Vicryl™Plus, braided, absorbable, Johnson & Johnson Medical GmbH, Ethicon Deutschland, Norderstedt, Germany). To protect the cover glass against manipulation by the rats, the observation window was covered with a lid, which was fixed by two screws. The rats were treated with antibiotics (enrofloxacin 5 mg/kg, Baytril 25 mg/ml, Bayer, Leverkusen, Germany) intraoperatively and per os for 7 days and with analgetics (carprofen, 5 mg/kg, Rimadyl 50 mg/ml, Pfizer Deutschland GmbH, Berlin) for 2 days after surgery. Postoperatively, the animals were given 3 days for convalescence and adaption to the femur chamber before insertion of the implant material. For implantation, the lid, the coverslip, and the cover glass were removed. In anaesthesia, the implant material was inserted in the centre of the observation window and fixed with the suture material, which had been placed around the femur during operation. For this purpose, the suture material is knotted over the implant. During the experimental period, the animals were evaluated daily with a score-based evaluation system including the assessment weight loss, general condition, spontaneous behaviour, clinical findings, and lameness.

2.7 | Intravital fluorescence microscopy

For intravital microscopic observation of the microcirculation, the animals were anaesthetized as described above, and the left hind limb

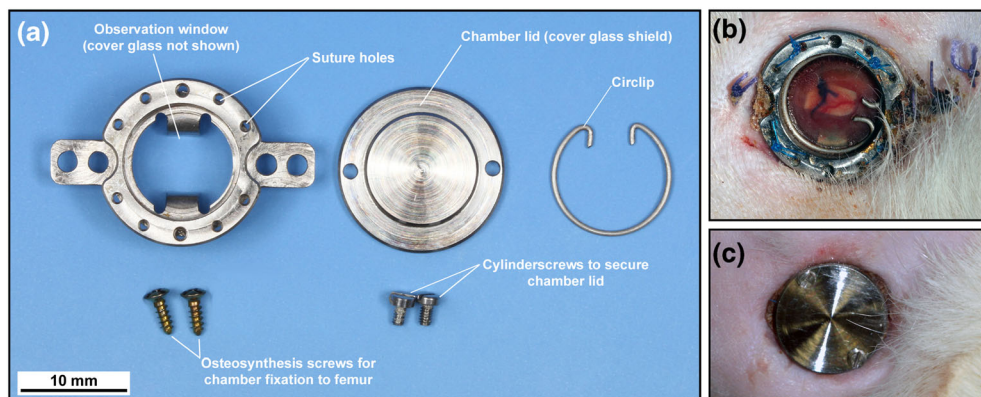


FIGURE 1 (a–c) Femur chamber. (a) The observation window (Ø10 mm) was fixed by two osteosynthesis screws to the bone and covered with a coverslip, which was secured by a circlip. The observation window was protected with a chamber lid, fixed with two cylinder screws to the chamber frame. (b) In vivo situation with an implant, which was fixed by suture material on the femur (chamber lid removed), 17 days after implantation. (c) In vivo situation with attached chamber lid 17 days after implantation [Colour figure can be viewed at wileyonlinelibrary.com]

was immobilized by a custom-made restraint device. Animals received an intravenous injection in the tail vein of 0.1 ml of 15% fluorescein-isothiocyanate-labelled dextran (FITC-dextran, MW 150,000; Sigma-Aldrich Chemie GmbH, Taufkirchen, Germany) in 0.9% NaCl (BBraun, Melsungen, Germany) for contrast enhancement of blood plasma and 0.1 ml of 0.1% rhodamine 6G (Sigma-Aldrich Chemie GmbH, Taufkirchen, Germany) in 0.9% NaCl (BBraun, Melsungen, Germany) for direct observation of leukocytes.

IVM was performed by using a modified Zeiss microscope (Axio Scope.A1, Carl Zeiss Microscopy GmbH, Göttingen, Deutschland), microscope equipped with a 120-W mercury lamp, and an illuminator with blue and green filter blocks (Zeiss Microscopy, Göttingen, Germany) for epi-illumination of the microcirculation of striated musculature. By using a charge-coupled device video camera (FK-7512-IQ, Pieper GmbH, Schwerte, Germany), the microscopic images were recorded and transferred to a Blu-ray recorder (JVC SR-HD 1700/EU, JVC Kenwood Deutschland GmbH, Bad Vilbel, Germany) for offline evaluation.

2.8 | Analysis of microcirculatory parameters

The recorded data were analysed by means of the image analysis software CapImage (CapImage 8.6.3., Zeintl, Heidelberg Germany). Leukocyte–endothelial cell interactions, microhaemodynamics, and macromolecular leakage were measured in four different regions of interest in the border zone of the scaffold by using 2.5×, 10×, and 20× objectives resulting in 90×, 370×, and 940× magnification on the monitor. In each region of interest, one venule in the granulation tissue around the implant (inner diameter: 20–40 µm) was selected and observed over 20 s for evaluation of vessel diameter, red blood cell velocity, wall shear rate, and macromolecular leakage. The leukocytes were classified according to their interaction with the vascular endothelium as adherent, rolling, or free flowing cells. Adherent leukocytes were cells that did not move or detach from the endothelial lining within an observation period of 20 s. Rolling leukocytes were moving cells with a velocity less than two fifth of the centreline velocity. Diameters (d) were analysed in micrometres perpendicular to the vessel path. The velocity (v) was measured using the line-shift method (T. Klyscz, 1997). Volumetric blood flow was calculated by $Q = \pi \times \left(\frac{d}{2}\right)^2 \times \frac{v}{1.6}$ [pl/s]. For correction of the parabolic velocity profile in microvessels, the Baker–Wayland factor 1.6 was used (Baker & Wayland, 1974). Based on the Newtonian definition, the wall shear rate was calculated by $\gamma = 8 \times \frac{v}{d}$. Macromolecular leakage was analysed by means of grey levels in the tissue directly adjacent to the venular vessel wall (E_1) and in the marginal cell free plasma layer within the blood vessel (E_2). Extravasation (E) was calculated as $E = E_1/E_2$. Microvessel density, defined as the length of blood vessels per area of observation given in cm/cm², was measured in the periphery around the implant and in the centre of the implant. Both values were displayed as the total functional capillary density expressed as the sum of peripheral and central functional capillary density.

2.9 | Histology and immunohistochemistry

At the end of the postoperative observation period of 20 days, animals were finalized via cervical dislocation under deep anaesthesia, and histological examinations were performed. Formalin-fixed specimens of the femur were embedded in Technovit 9100 (Willbold & Witte, 2010). Thin sections (5 µm) were stained with haematoxylin (Merck KGaA, Darmstadt, Germany) and eosin (Merck KGaA, Darmstadt, Germany) according to standard procedures. For histochemical detection of collagen fibres, we performed van Gieson staining of thin sections (5 µm) with haematoxylin (Merck KGaA, Darmstadt, Germany) and picrofuchsin acid solution (Merck KGaA, Darmstadt, Germany) according to standard procedures. All specimens were examined by light microscopy (Leica DM4000 B, Leica Mikrosysteme, Wetzlar, Germany).

For detection of capillaries, endothelial cells were immunohistochemically stained using a rabbit anti-rat CD34 antibody (Hoelzel Diagnostika Handels GmbH, Koeln, Germany). As a secondary antibody, a biotin conjugated antibody (DIANOVA GmbH, Hamburg, Germany) was used. After incubation with streptavidin-horseradish peroxidase (DIANOVA GmbH, Hamburg, Germany), the colour development after addition of 3,3'-diaminobenzidine (Vector Laboratories, Inc., Burlingame, CA, USA) was monitored microscopically followed by counterstaining with haematoxylin. By omitting the primary antibody step, negative controls were performed, which all showed no detectable staining.

By means of the marker enzyme, naphthol-AS-D-chloroacetate-esterase neutrophilic granulocytes were determined. Sections were first washed in distilled water and then incubated with naphthol AS-D chloroacetate (Sigma, Taufkirchen, Germany) in 4% pararosaniline (Chroma, Olching, Germany) and 4% sodium nitrate in 0.1M acetate buffer for 120 min. Sections were washed in distilled water and mounted with Aquatex (Merck). Cells containing red-brownish granules were regarded as positive. Control sections were incubated without the substrate. No staining developed in these controls.

2.10 | Statistics

Results are expressed as means ± standard error of the mean (SEM). Differences between groups were assessed by one-way analysis of variance (ANOVA), and differences within groups were analysed by one-way repeated measures ANOVA. To isolate differences between pairs of groups, Student–Newman–Keuls post hoc tests were performed. Differences were considered significant at $p < .05$.

3 | RESULTS

3.1 | Properties of the material

The control group (porous polymer patch) showed very large pore sizes of up to 175.34 µm and a high porosity (Table 1). Produced PCL fibre mats show a non-aligned structure as it can be seen in

TABLE 1 Fibre diameter in μm , porosity in %, maximum pore diameter in μm , middle pore diameter in μm , and smallest pore diameter in μm of the control group scaffold (control), the unmodified PCL fibre mat group (PCL), and PCL fibre mat modified with a special fibre modification utilizing chitosan group (CS-g-PCL)

	Control	PCL	CS-g-PCL
Fibre diameter (μm)	—	2.218 \pm 0.516	2.421 \pm 0.501
Porosity (%)	94.7	80.61	76.21
Maximum pore diameter (μm)	175.34	9.19	8.16
Middle pore diameter (μm)	139.43	6.97	6.52
Smallest pore diameter (μm)	78.14	3.81	4.71

Abbreviation: PCL, polycaprolactone.

SEM images (Figure 2). It was found that the pure PCL had a porosity of 80.61%. The maximum pore size (9.19 μm) was considerably lower than for the control group (Table 1). Modification with the graft-copolymer CS-g-PCL reduced the porosity to 76.21% and simultaneously increased the fibre diameter (Table 1). This observation was to be expected when applying a surface coating by crystallization to the electrospun PCL fibres.

3.2 | Animals

The animals showed no signs of discomfort or changes in behaviour. Immediately after anaesthesia, the operated limbs were loaded again. In the control group 1, animal was lost because of weight loss. In the PCL group 1, animal was lost because of failure of chamber fixation. In the CS-g-PCL group 3, animals were lost because of anaesthesia and weight loss. These animals were not included in the statistical evaluation.

3.3 | Microhaemodynamic parameters

First, immediately after implantation and on Day 3, microhaemodynamic parameters were not detectable by means of IVM. The collected data including the diameter, the volumetric blood flow, and the wall shear rate indicated that the different implant materials interfered with the microvascular blood flow of host tissue.

Venular diameters stayed constant in all experimental groups ranging between 14 and 19 μm (Table 2). Volumetric blood flow and wall shear rates of venules were not significantly altered (Table 2).

3.4 | Functional capillary density

Immediately after implantation and on Day 3, capillaries were not observable by means of IVM. On Day 6, first results were visible in the PCL group; however, in the other groups, no capillaries were observed. The functional capillary density in the PCL group stayed nearly constant over the evaluation period. The functional capillary density caused by the control implant was comparable with that provoked by the implantation of the unmodified fibre mat (PCL) and showed a slight increase up to Day 14. This process stagnated at Days 17 and 20. In the CS-g-PCL group, we observed a significant increase in functional capillary density at Day 10 compared with Day 6. At Day 14, the functional capillary density caused by the implantation of CS-g-PCL was significantly increased compared with the control group and the PCL group. At Days 17 and 20, the capillary density of CS-g-PCL decreased and was at the level of the control and PCL (Figure 3).

3.5 | Inflammatory response

Evaluation of leukocyte endothelial interaction started at Day 6, because they were not observable at earlier time points. The used scaffolds induced only limited differences in leukocyte reaction between the groups. In the PCL group, the number of rolling leukocytes was significantly increased at Day 10 compared with the control group and CS-g-PCL group. Afterwards, the number of rolling leukocytes in the PCL group was decreased at Day 14 and stayed constant until Day 20. The CS-g-PCL group showed nearly constant values from Day 10 to Day 20 (Figure 4a). The number of adherent leukocytes in the control group increased from Day 10 to Day 14. The control group also showed a significant increase of adherent leukocytes compared with the groups PCL and CS-g-PCL at Day 14. In this group, the adherent leukocytes decreased at Day 17 and stayed almost constant until Day 20. The number of adherent leukocytes that was observed for the PCL group showed a variable course during the evaluation period. There was an increase from Day 6 to Day 10, a steep

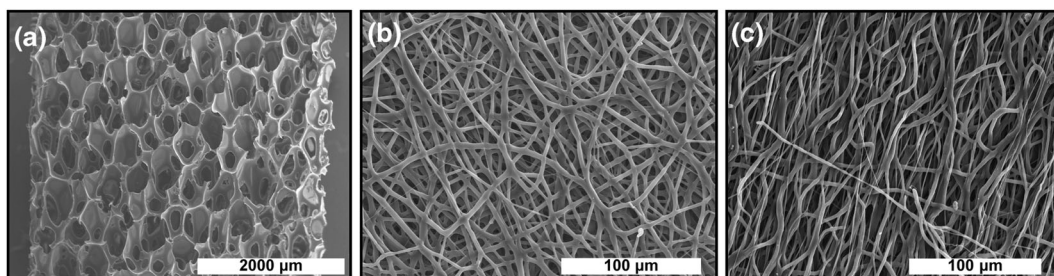


FIGURE 2 Scanning electron microscope micrographs of (a) the porous polymer patch (control group), (b) the unmodified polycaprolactone fibre mat, and (c) the CS-g-PCL fibre mat

TABLE 2 Venular diameters in μm , volumetric blood flow in pl/s , and wall shear rate in s^{-1} of postcapillary and collecting venules at the border zones of the porous polymer patch control group (control), the unmodified PCL fibre mat group (PCL), and the chitosan-modified PCL fibre mat group (CS-g-PCL) 6, 10, 14, 17, and 20 days after implantation

	Day 6	Day 10	Day 14	Day 17	Day 20
Diameter (μm)					
Control	14.5 \pm 0.0	18.2 \pm 1.1	16.8 \pm 1.4	15.9 \pm 1.0	15.6 \pm 1.4
PCL	17.0 \pm 1.5	16.4 \pm 0.9	17.2 \pm 1.4	18.0 \pm 1.2	16.6 \pm 1.5
CS-g-PCL	14.0 \pm 0.0	15.7 \pm 1.5	18.9 \pm 0.8	7.4 \pm 7.3	15.0 \pm 1.5
Shear rate (s^{-1})					
Control	159.5 \pm 0.0	236.0 \pm 9.0	294.8 \pm 30.0	245.8 \pm 38.0	239.0 \pm 62.4
PCL	137.6 \pm 33.9	228.0 \pm 49.6	141.3 \pm 26.6	144.8 \pm 28.7	120.0 \pm 19.2
CS-g-PCL	174.6 \pm 0.0	134.5 \pm 39.1	181.9 \pm 41.1	281.1 \pm 0.0	232.1 \pm 9.7
Volumetric blood flow (pl/s)					
Control	30.1 \pm 0.0	88.7 \pm 15.1	90.6 \pm 22.8	58.6 \pm 7.8	53.2 \pm 13.7
PCL	45.9 \pm 16.6	59.5 \pm 12.8	56.6 \pm 23.7	61.7 \pm 24.2	32.9 \pm 5.9
CS-g-PCL	29.3 \pm 0.0	32.7 \pm 10.3	79.8 \pm 22.1	54.7 \pm 0.0	51.2 \pm 13.2

Note. Values are expressed as means \pm SEM.

Abbreviation: PCL, polycaprolactone.

decrease at Day 14, and again an increase until Day 20, which reached nearly the value present at Day 10. In the CS-g-PCL group, adherent leukocytes could be observed beginning with Day 10. Compared with the control group and the PCL group, the results were lower at Days 10 and 14, but from Day 10 to Day 17, there was an increase in the number of adherent leukocytes. At Day 20, the adherent leukocytes decreased in the CS-g-PCL group (Figure 4b).

3.6 | Histology and immunohistochemistry

Haematoxylin–eosin-staining showed obvious differences in cell infiltration depending on the implant material. Infiltration with cells appeared uniform in the control group. In the PCL group, however, ingrowth of cells was also detectable, but to a lesser extent compared with the control group. The PCL group showed a clear cellular margin with a kind of encapsulation (Figure 5e). In the CS-g-PCL group, the histological findings were comparable, but there was barely no margin around the implant present (Figure 5a–f).

Collagen fibres were visualized by van Gieson staining (Figure 5g–i). Collagen fibres were histologically representable in the control group as well as in the experimental groups. The control group showed an equal distribution of orientated collagen fibres around the implant structure. The PCL group showed collagen fibres especially in the border area of the implant, which were less prominent compared with the control group. In the CS-g-PCL group, only a few collagen fibres around the implant could be demonstrated.

A semiquantitative analysis of foreign body giant cells (FBGC; Figure S1) revealed the highest number of FBGC around the unmodified PCL implants. In the control group and the CS-G-PCL group, the count of FBGC was comparably low.

Immunohistochemical examination with CD34-based detection of vascular structures at Day 20 was applied to verify the results obtained with IVM. Highly vascularized granulation tissue around the implant was detectable in the control group and the group with CS-g-PCL fibre mats. The unmodified PCL fibre mats were surrounded by granulation tissue, which showed a lower vessel density. It should be emphasized that in the CS-g-PCL group, vessels within the implant material were also detectable (Figure 5d–f), which was not the case for the PCL group. To further characterize the cellular margin visible around the PCL fibre mats, a naphthol-AS-D-chloracetate-esterase staining was applied to detect neutrophilic granulocytes. This cell type was present in all groups, but especially the PCL fibre mats (PCL and CS-g-PCL) showed a high infiltration of neutrophilic granulocytes (Figure 6).

4 | DISCUSSION

In this study, using the femur chamber in rats, we demonstrated that CS-g-PCL modification of PCL fibre mats improved angiogenesis in vivo. Currently, tissue regeneration after defects independent of the field of application is limited by the absence of proven strategies for the generation of adequately vascularized tissues (Schumann et al., 2011). Sufficient perfusion is important for oxygen supply, nutrition of cells and tissues when cellular ingrowth in scaffolds shall be achieved, and for removal of metabolites (Lovett et al., 2009). Therefore, it is of great importance to gather knowledge about the extent and time course of vascularization of different implant materials before they can be successfully used in a clinical setting (Laschke et al., 2006).

The modification of the PCL fibre mats with CS-g-PCL showed a marked improvement in angiogenesis in the first 2 weeks after

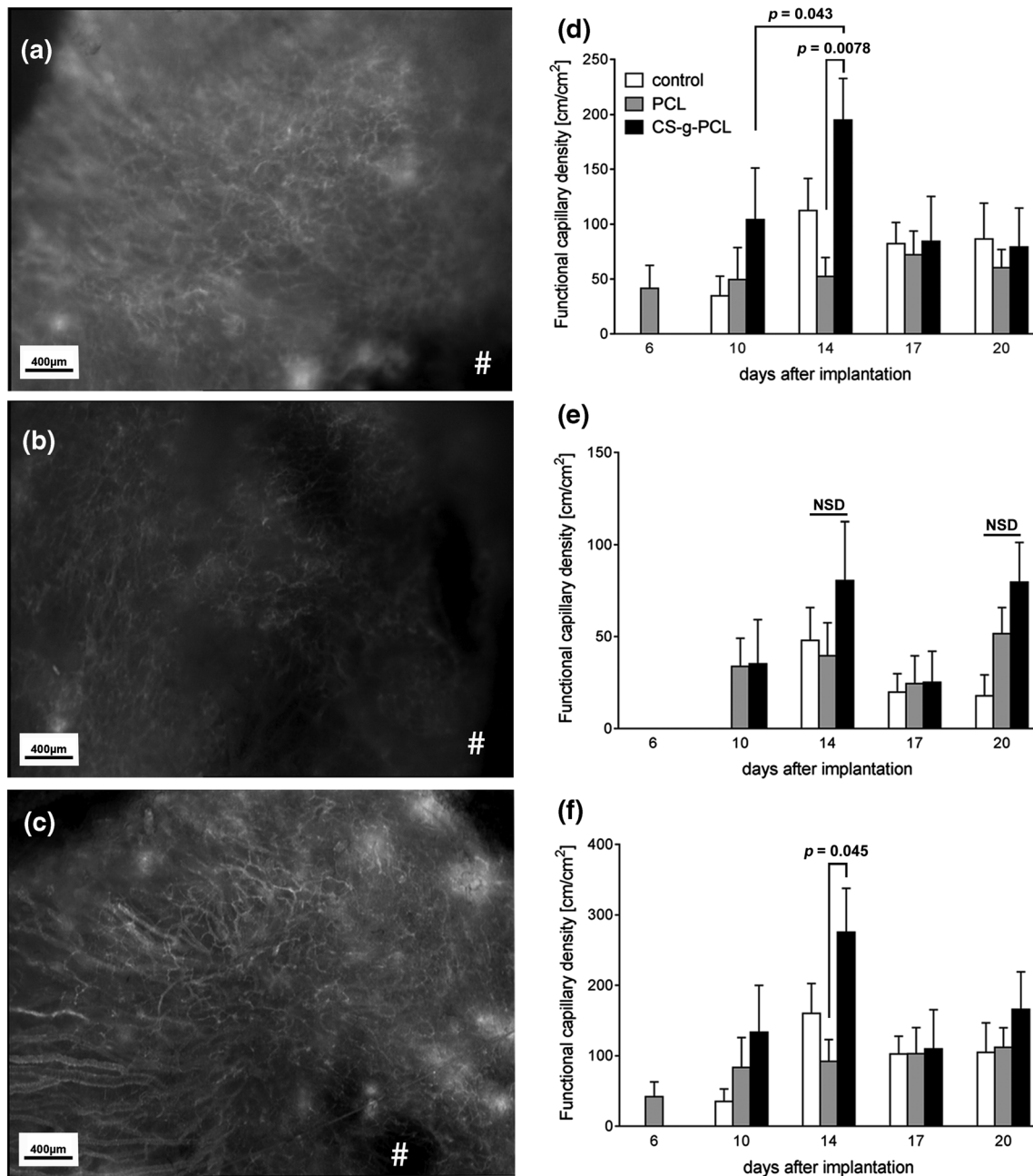


FIGURE 3 Neovascularization in the femur chamber model: (a–c) Representative intravital fluorescence microscopy overview images of (a) control, (b) polycaprolactone, and (c) CS-g-PCL 20 days after implantation. The centres of the implants are marked (#). (d–f) Quantification of neovascularization expressed as functional capillary density in cm/cm^2 (d) in the border zones of the implants, (e) in the centre of the implants, and (f) total functional capillary density expressed as the sum of peripheral and central functional capillary density. All values in this figure represent the mean \pm SEM

implantation compared with the unmodified mats and the control group. Particularly in the early phase, rapid development of vessels for supply of ingrowing cells is important. Only then the survival of the immigrant cells and thus the survival of the implant secured. Vessels were detected at Day 6 onwards in this model although angiogenesis was expected to start sooner (Carmeliet, 2000; Ke & Costa, 2006). Studies in the dorsal skinfold chamber in mice and hamsters showed that angiogenesis already had increased on Day 3 (Zimmerer et al., 2017). Whereas in the femur chamber in mice, which is a hard tissue

model and therefore maybe the better comparison, results on angiogenesis were also obtained from Day 6 (Tavassol et al., 2011). Angiogenesis is the complex and tightly regulated process of formation of new capillaries from existing blood vessels (Laschke et al., 2006). After an injury, acute necrosis and hypoxia occur in the affected area. The local oxygen concentration regulates the expression of the angiogenic factor VEGF via hypoxia-inducible factor-1 α (Laschke et al., 2006; Norrby, 1997). A reason for the finding that we could observe first signs of angiogenesis beginning from Day 6 might be the surgical

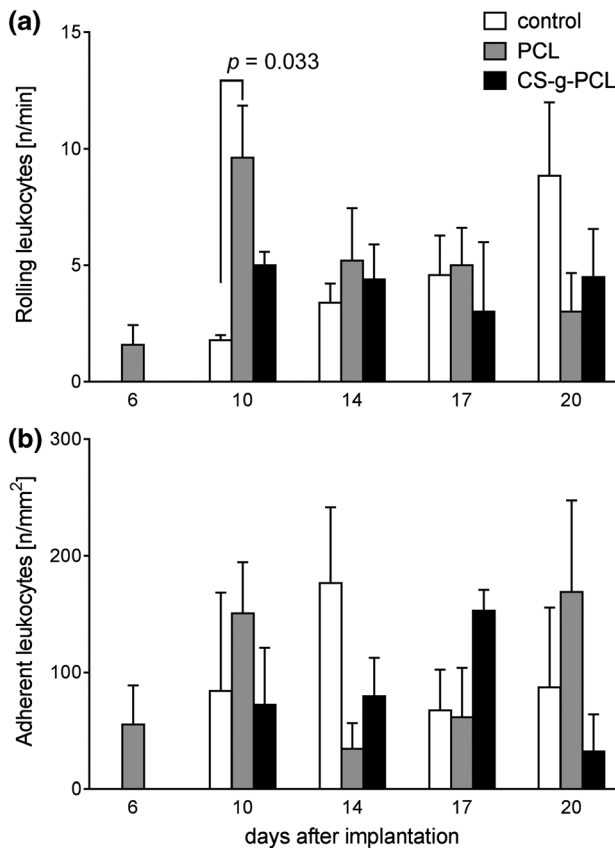


FIGURE 4 Leukocyte–endothelium interaction at the periphery of the implants in postcapillary and collecting venules after implantation. (a) Number of rolling leukocytes 6, 10, 14, 17, and 20 days after implantation shown as number of cells/min. (b) Number of adherent leukocytes 6, 10, 14, 17, and 20 days after implantation shown as number of cells/mm². All values in this figure represent the mean \pm SEM

procedure. Compared with the dorsal skinfold chamber, the preparation of the femur chamber is more invasive; therefore, a longer regeneration period after preparation of the chamber is needed. Within the chamber, blood and debris must be removed before vessels were observable. The course of the functional capillary density showed a good vascular supply from Day 10 to Day 14 after implantation. The decline from Day 17 is explainable considering the growth and development of vessels by the beginning of a remodelling process, which results later in the formation of a structured network of vessels (Carmeliet, 2000). By determining the functional capillary density in the length of the vessels per area, this results in a smaller value. Many small vessels were measured by Day 14. By remodelling the intravital microscopic examination showed fewer but larger vessels.

Modification of PCL with chitosan is often used to enhance biocompatibility of PCL-based scaffolds for different tissue engineering approaches. This can be achieved either by first modifying the polymers and generating scaffolds via electrospinning as a consecutive step (Chen, Huang, Yu, Liu, & Gu, 2011) or, as with the CS-g-PCL scaffold in this study, as a secondary modification after electrospinning of PCL. This modification resulted in an increased *in vitro* biocompatibility in terms of enhanced cell attachment and growth compared with

uncoated PCL fibre mats (de Cassan et al., 2018). In the present study, these data were supported by our *in vivo* data in reference to biocompatibility and angiogenesis. In contrast to the PCL group, which showed a prominent fibrous capsule, the CS-g-PCL group showed only a minor deposition of collagen fibres around the implant and the lowest amount of FBGC proving the good biocompatibility achieved by the chitosan modification. The number of FBGC was comparable in the control group, but there was a higher deposition collagen with orientated fibres, which may be a hint of a stronger foreign body reaction. With respect to the short observation period after implantation, this is just a hypothetical assumption, which should be proven in further studies.

Although we could show an enhanced angiogenesis as a reaction to the implantation of PCL-based scaffolds, there is still a lack of vessels inside the PCL-based scaffolds. Only in the CS-g-PCL group vessels were detectable inside the scaffold. A crucial factor for the vascularization of implants and the ingrowth of cells is the porosity of the implant. In a study using the mice skinfold chamber model and intravital microscopy, a pore size of approximately 250–300 μ m was found to promote the best vascularization of poly(ether ester) block-copolymer scaffolds (Druecke et al., 2004). In this study, the authors also showed that the effect of pore size is more prominent in the centre of the implant. Implants with a larger pore size showed a higher functional capillary density in the border zone at early time points, but later, there was no difference between the different pore sizes observable. This effect is also present in our study: At later time points, the functional capillary density is comparable in all groups in the border zone of the implants. At the centre of the implants, we observed differences between the groups also at later time points. Taking the development of the granulation tissue into account, this result can be explained. We assume that development of the granulation tissue originated from the tissue underneath the implants resulting in a faster growth in the border zone of the implants. Because of the larger pore size, tissue growth through the pores of the implants was only observed to a larger extent in the control group. In the CS-g-PCL group, we detected a limited ingrowth of capillaries, whereas we detected no vascular ingrowth into the implants of the PCL group. From this observation, one would assume that the functional capillary density in the centre will reach the highest value in the control group, but our results showed that functional density in the centre reached the highest values in the CS-g-PCL group. This finding reflects the good biocompatibility of these implants accomplished by the chitosan modification and may be due to an accelerated growth of granulation tissue that rapidly enwrapped the implant. Further developments of the CS-PCL scaffolds may be needed to further enhance the ingrowth of vessels. To achieve this aim, various approaches are possible. One possibility is the addition of angiogenic growth factors, which trigger vessel growth. Release of VEGF from porous PCL-based scaffolds caused an enhancement of angiogenesis, which led to a higher ingrowth of vessels into depth of the scaffold (Singh, Wu, & Dunn, 2012), and more mechanistic approaches are possible. Vascularization of scaffolds depends to a large extent on the accessibility of the inner parts of the scaffold for growing vessels.

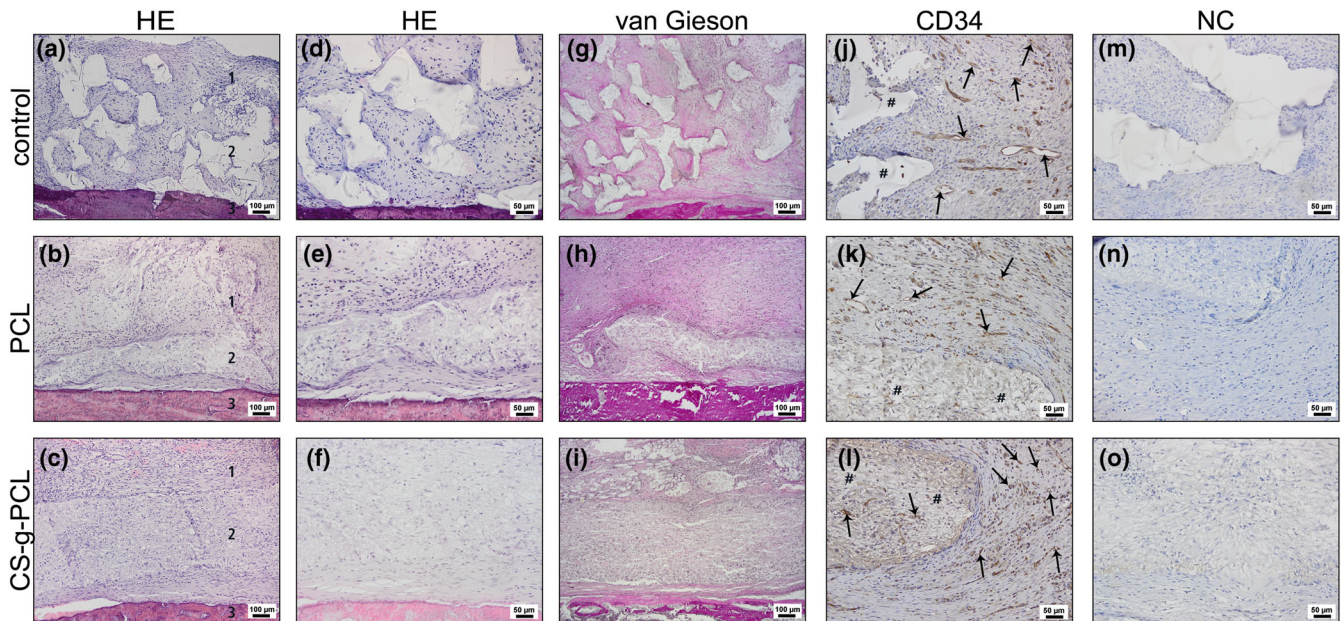


FIGURE 5 HE staining, van Gieson staining, and immunohistochemical detection of CD 34: Representative histological stainings (a–o) 20 days after implantation into the femur chamber in Lewis rats. (a–c) HE staining of (1) granulation tissue, (2) implant, and (3) bone. (d–f) HE staining with higher magnification. (g–i) Collagen fibres were detected by van Gieson staining. (j–l) The presence of endothelial cells and accordingly the presence of vascular structures were confirmed by immunohistochemical detection of CD34. (m–o) Negative controls. Areas of the implant are marked (#), and arrows denote vascular structures [Colour figure can be viewed at wileyonlinelibrary.com]

With respect to electrospun scaffolds, an increase in pore size can be achieved via the inclusion of sacrificial fibres of a water soluble polymer during the spinning process (Phipps, Clem, Grunda, Clines, & Bellis, 2012). These fibres were removed after production of the scaffold leading to a larger mean pore size, which in turn facilitates the ingrowth of cells. Larger pores can be generated by means of laser cutting. Increasing diameters of pores enhanced the vascularization of scaffolds and in turn resulted in a better cellular infiltration (Joshi, Lei, Walthers, Wu, & Dunn, 2013). This effect is also influenced by the overall porosity. The higher the content of macropores was, the more blood vessels inside the scaffold and infiltrating cells could be detected (Walthers, Nazemi, Patel, Wu, & Dunn, 2014). With regard to our study, we assume that a further enhancement of angiogenesis and particularly of cell infiltration into the CS-g-PCL scaffold could be induced by enhancing the porosity and pore size of the scaffold. This could be achieved via the generation of macropores or by using larger fibre diameters, which in turn also will result in enhanced mechanical properties of the scaffolds, as was shown by Wang et al. (2014).

Different models for assessing the angiogenic and inflammatory reaction after the implantation of different materials have been established so far. Most of these models are performed using mice (Burghartz et al., 2015) or rats (Seyednejad et al., 2012) and are characterized by a final point at which the samples are examined. However, these end point models cannot generate any information regarding the changes in the vasculature over the time course of the experiment. To explore the angiogenic and inflammatory reaction of soft tissues, the dorsal skinfold chamber is a widely used model (Kampmann et al., 2013). As a comparable model for the investigation

of vascularization and biocompatibility in hard tissues, the femur chamber in mice, which allowed to place implants in the immediate environment of the femur, was established (Tavassol et al., 2011). In the present study, we used a model, which was adapted to the femur of rats. In contrast to the mouse femur chamber in the rat model, no bone defect was created. Instead, the implant was fixed by means of suture material to the bone. The area in which the trochanter major was removed is only for fixation of the chamber and is not in the observation window. There was no bone defect in the observation area in the bone. This preparation method may have affected the measured parameters, as the periosteum may be injured by manipulation during surgery. Nevertheless, the results provide important information about vascularization of implants in bony environment, because even in patients, the periosteum may already be injured by rupture of the tendon or is damaged during surgical procedure. The femur chamber was characterized by an observation chamber, which permitted a steady microscopic view of the implanted scaffold without disturbance of the growing tissue and therefore the study of the hard tissue reaction repeatedly in the same animal over an evaluation period of 20 days. Furthermore, by recording leucocyte endothelial interactions, we could also generate data about the local inflammatory response to the scaffold implantation, which is also not possible with standard end point models.

As a control group, a commercial porous polymer patch was used, which has a proven biocompatibility. Despite the fact that the material parameters of the control group markedly differ from experimental groups, this material was chosen, because earlier studies confirmed the improvement of mechanical properties using this patch for rotator cuff tear repair (Ricchetti, Aurora, Iannotti, & Derwin, 2012). In the

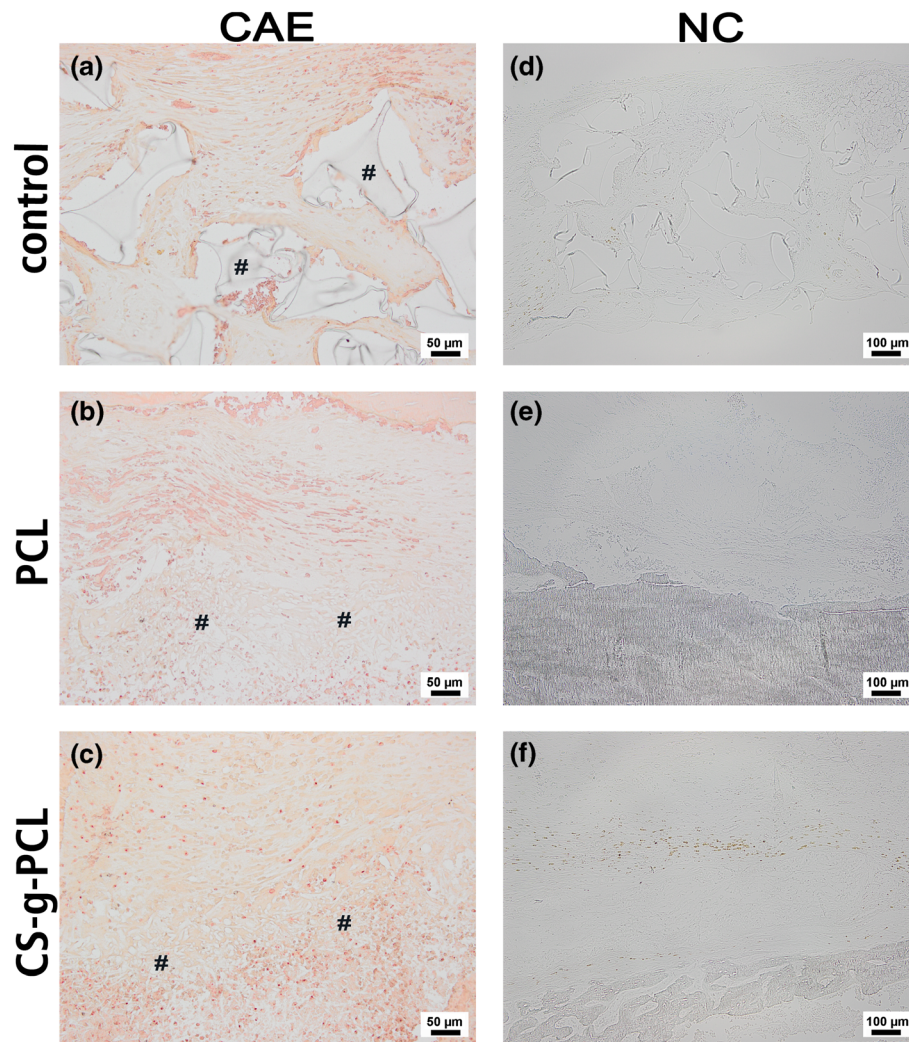


FIGURE 6 Chloracetate-esterase staining for detection of neutrophilic granulocytes: Representative histological stainings 20 days after implantation into the femur chamber in rats (#) implant [Colour figure can be viewed at wileyonlinelibrary.com]

experimental groups, PCL, which is well known for its biocompatibility, was used to fabricate electrospun fibre mats. During electrospinning, undirected fibres were produced mimicking the structure of unaligned collagen fibres of the bone. In addition, the process of electrospinning increased the mechanical stability, because unprocessed PCL is not sufficient for load bearing applications (Agrawal & Ray, 2001).

In conclusion, graft copolymer modification showed improved vascularization compared with the unmodified material. The approach of this study is promising for clinical use of CS-g-PCL-based implants in various clinical applications, after further examination of the CS-g-PCL implants in small and large animals.

ACKNOWLEDGEMENTS

This research project has been supported by the DFG FOR 2180 “Gradierte Implantate für Sehnen-Knochen-Verbindungen” (KA 4236/1-1). We acknowledge the excellent technical assistance of Stefanie Rausch.

CONFLICT OF INTEREST

The authors confirm that there are no known conflicts of interest associated with this study.

ORCID

Elmar Willbold  <https://orcid.org/0000-0002-3713-9255>

Andreas Kampmann  <https://orcid.org/0000-0003-1904-5965>

REFERENCES

- Agrawal, C. M., & Ray, R. B. (2001). Biodegradable polymeric scaffolds for musculoskeletal tissue engineering. *Journal of Biomedical Materials Research*, 55, 141. [https://doi.org/10.1002/1097-4636\(200105\)55:2<141::AID-JBM1000>3.0.CO;2-J-150](https://doi.org/10.1002/1097-4636(200105)55:2<141::AID-JBM1000>3.0.CO;2-J-150).
- Apostolakos, J., Durant, T. J., Dwyer, C. R., Russell, R. P., Weinreb, J. H., Alae, F., ... Mazzocca, A. D. (2014). The enthesis: A review of the tendon-to-bone insertion. *Muscles, Ligaments and Tendons Journal*. CIC Edizioni Internazionali, 4(3), 333–342. Available at: <http://www.ncbi.nlm.nih.gov/pubmed/25489552>. Accessed: 27 February 2018

- Baker, M., & Wayland, H. (1974). On-line volume measurement flow rate and velocity profile for blood in microvessels. *Microvascular Research*, 7, 131–143. [https://doi.org/10.1016/0026-2862\(74\)90043-0](https://doi.org/10.1016/0026-2862(74)90043-0)
- Boileau, P., Brassart, N., Watkinson, D. J., Carles, M., Hatzidakis, A. M., & Krishnan, S. G. (2005). Arthroscopic repair of full-thickness tears of the supraspinatus: Does the tendon really heal? *Journal of Bone and Joint Surgery - Series A*, 87, 1229. <https://doi.org/10.2106/JBJS.D.02035>
- Burghartz, M., Gehrke, T., Storck, K., Staudenmaier, R., Mandlik, V., Schurr, C., ... Kleinsasser, N. (2015). Vascularization of engineered cartilage constructs in a mouse model. *Cell and Tissue Research*, 359(2), 479–487. <https://doi.org/10.1007/s00441-014-2026-2>
- Carmeliet, P. (2000). Mechanisms of angiogenesis and arteriogenesis. *Nature Medicine*, 6(4), 389–395. <https://doi.org/10.1038/74651>
- Chen, H., Huang, J., Yu, J., Liu, S., & Gu, P. (2011). Electrospun chitosan-graft-poly(ϵ -caprolactone)/poly(ϵ -caprolactone) cationic nanofibrous mats as potential scaffolds for skin tissue engineering. *International Journal of Biological Macromolecules*, 48(1), 13–19. <https://doi.org/10.1016/j.ijbiomac.2010.09.019>
- Dash, T. K., & Konkimalla, V. B. (2012). Poly- ϵ -caprolactone based formulations for drug delivery and tissue engineering: A review. *Journal of Controlled Release*, 158(1), 15–33. <https://doi.org/10.1016/j.jconrel.2011.09.064>
- de Cassan, D., Sydow, S., Schmidt, N., Behrens, P., Roger, Y., Hoffmann, A., ... Menzel, H. (2018). Attachment of nanoparticulate drug-release systems on poly(ϵ -caprolactone) nanofibers via a graftpolymer as interlayer. *Colloids and Surfaces. B, Biointerfaces Elsevier*, 163, 309–320. <https://doi.org/10.1016/J.COLSURFB.2017.12.050>
- Druecke, D., Langer, S., Lamme, E., Pieper, J., Ugarkovic, M., Steinau, H. U., & Homann, H. H. (2004). Neovascularization of poly (ether ester) block-copolymer scaffolds in vivo: Long-term investigations using intravital fluorescent microscopy. *Journal of Biomedical Materials Research. Part A*, 68(1), 10–18. <https://doi.org/10.1002/jbm.a.20016>
- Encalada-Diaz, I., Cole, B. J., MacGillivray, J. D., Ruiz-Suarez, M., Kercher, J. S., Friel, N. A., & Valero-Gonzalez, F. (2011). Rotator cuff repair augmentation using a novel polycarbonate polyurethane patch: Preliminary results at 12 months' follow-up. *Journal of Shoulder and Elbow Surgery*, 20(5), 788. <https://doi.org/10.1016/j.jse.2010.08.013>
- Ferracini, R., Martínez Herreros, I., Russo, A., Casalini, T., Rossi, F., & Perale, G. (2018). Scaffolds as structural tools for bone-targeted drug delivery. *Pharmaceutics*, 10(3), 1–26. <https://doi.org/10.3390/pharmaceutics10030122>
- Font Tellado, S., Balmayor, E. R., & Griensven, M. (2015). Strategies to engineer tendon/ligament-to-bone interface: Biomaterials, cells and growth factors. *Advanced Drug Delivery Reviews Elsevier*, 94, 126–140. <https://doi.org/10.1016/J.ADDR.2015.03.004>
- Fu, X., Sammons, R. L., Bertóti, I., Jenkins, M. J., & Dong, H. (2011). Active screen plasma surface modification of polycaprolactone to improve cell attachment'. *Journal of Biomedical Materials Research Part B: Applied Biomaterials*. Wiley-Blackwell, 100B(2), 314–320. <https://doi.org/10.1002/jbm.b.31916>
- Gerber, C., Meyer, D. C., Frey, E., von Rechenberg, B., Hoppeler, H., Frigg, R., ... Zumstein, M. A. (2009). Neer Award 2007: Reversion of structural muscle changes caused by chronic rotator cuff tears using continuous musculotendinous traction. An experimental study in sheep. *Journal of Shoulder and Elbow Surgery*, 18, 163. <https://doi.org/10.1016/j.jse.2008.09.003-171>
- Gerber, C., Meyer, D. C., Schneeberger, A. G., Hoppeler, H., & Von Rechenberg, B. (2004). Effect of tendon release and delayed repair on the structure of the muscles of the rotator cuff: An experimental study in sheep. *The Journal of Bone and Joint Surgery. American*, 86-A(9), 1973–1982. doi: 86/9/1973 [pii]
- Giai Via, A., De Cupis, M., Spoliti, M., & Oliva, F. (2013). Clinical and biological aspects of rotator cuff tears. *Muscles, Ligaments and Tendons Journal*, 3(2), 70–79. Available at: <https://www.ncbi.nlm.nih.gov/pmc/articles/PMC3711705/pdf/70-79.pdf>. Accessed: 27 February 2018
- Gulotta, L. V., Kovacevic, D., Packer, J. D., Deng, X. H., & Rodeo, S. A. (2011). Bone marrow-derived mesenchymal stem cells transduced with scleraxis improve rotator cuff healing in a rat model. *The American Journal of Sports Medicine*, 39(6), 1282–1289. <https://doi.org/10.1177/0363546510395485>
- Jena, A., & Gupta, K. (2001). An innovative technique for pore structure analysis of fuel cell and battery components using flow porometry. *Journal of Power Sources*, 96, 214–219. [https://doi.org/10.1016/S0378-7753\(00\)00684-4](https://doi.org/10.1016/S0378-7753(00)00684-4)
- Joshi, V. S., Lei, N. Y., Walthers, C. M., Wu, B., & Dunn, J. C. (2013). Macroporosity enhances vascularization of electrospun scaffolds. *The Journal of Surgical Research*, 183(1), 18–26. <https://doi.org/10.1016/j.jss.2013.01.005>
- Jost, B., Zumstein, M., Pfirrmann, C. W., & Gerber, C. (2006). Long-term outcome after structural failure of rotator cuff repairs. *Journal of Bone and Joint Surgery - Series A*, 88, 472. <https://doi.org/10.2106/JBJS.E.00003>
- Kampmann, A., Lindhorst, D., Schumann, P., Zimmerer, R., Kokemüller, H., Rücker, M., ... Tavassol, F. (2013). Additive effect of mesenchymal stem cells and VEGF to vascularization of PLGA scaffolds. *Microvascular Research Academic Press*, 90, 71–79. <https://doi.org/10.1016/J.MVR.2013.07.006>
- Ke, Q., & Costa, M. (2006). Hypoxia-inducible factor-1 (HIF-1). *Molecular Pharmacology*, 70(5), 1469 LP–1480. Available at: <http://molpharm.aspetjournals.org/content/70/5/1469.abstract>
- Klyszcz, T. (1997). Cap image-a new kind of computer-assisted video image analysis system for dynamic capillary microscopy. *Biomedizinische Technik. Biomedical Engineering*, 42, 168–175. <https://doi.org/10.1515/bmte.1997.42.6.168>
- Lam, C. X. F., Hutmacher, D. W., Schantz, J. T., Woodruff, M. A., & Teoh, S. H. (2008). Evaluation of polycaprolactone scaffold degradation for 6 months in vitro and in vivo. *Journal of Biomedical Materials Research - Part A*, 90, 906. <https://doi.org/10.1002/jbm.a.32052-919>
- Laschke, M. W., Harder, Y., Amon, M., Martin, I., Farhadi, J., Ring, A., ... & Häufel, J. M. (2006). Angiogenesis in tissue engineering: Breathing life into constructed tissue substitutes. Available at: <http://online.liebertpub.com/doi/pdfplus/10.1089/ten.2006.12.2093> (Accessed: 27 February 2018).
- Li, D., Frey, M. W., & Joo, Y. (2006). Characterization of nanofibrous membranes with capillary flow porometry. *Journal of Membrane Science*, 286, 104–114. <https://doi.org/10.1016/j.memsci.2006.09.020>
- Lovett, M., Lee, K., Edwards, A., & Kaplan, D. L. (2009). Vascularization strategies for tissue engineering. *Tissue Engineering. Part B, Reviews*. Mary Ann Liebert, Inc., 15(3), 353–370. <https://doi.org/10.1089/ten.TEB.2009.0085>
- Lu, H. H., & Thomopoulos, S. (2013). Functional attachment of soft tissues to bone: Development, healing, and tissue engineering. *Annual Review of Biomedical Engineering NIH Public Access*, 15, 201–226. <https://doi.org/10.1146/annurev-bioeng-071910-124656>
- Meyer, D. C., Gerber, C., von Rechenberg, B., Wirth, S. H., & Farshad, M. (2011). Amplitude and strength of muscle contraction are reduced in experimental tears of the rotator cuff. *The American Journal of Sports Medicine*, 39, 1456–1461. <https://doi.org/10.1177/0363546510396305>

- Meyer, D. C., Wieser, K., Farshad, M., & Gerber, C. (2012). Retraction of supraspinatus muscle and tendon as predictors of success of rotator cuff repair. *The American Journal of Sports Medicine*, 40, 2242–2247. <https://doi.org/10.1177/0363546512457587>
- Nair, L. S., & Laurencin, C. T. (2007). Biodegradable polymers as biomaterials. *Progress in Polymer Science*, 32(8), 762–798. <https://doi.org/10.1016/j.progpolymsci.2007.05.017>
- Norrbj, K. (1997). Angiogenesis: New aspects relating to its initiation and control. *APMIS Wiley Online Library*, 105(1–6), 417–437. <https://doi.org/10.1111/j.1699-0463.1997.tb00590.x>
- Phipps, M. C., Clem, W. C., Grunda, J. M., Clines, G. A., & Bellis, S. L. (2012). Increasing the pore sizes of bone-mimetic electrospun scaffolds comprised of polycaprolactone, collagen I and hydroxyapatite to enhance cell infiltration. *Biomaterials*, 33(2), 524–534. <https://doi.org/10.1016/j.biomaterials.2011.09.080>
- Ricchetti, E. T., Aurora, A., Iannotti, J. P., & Derwin, K. A. (2012). Scaffold devices for rotator cuff repair. *Journal of Shoulder and Elbow Surgery Mosby*, 21(2), 251–265. <https://doi.org/10.1016/J.JSE.2011.10.003>
- Rodeo, S. A. (2007). Biological augmentation of rotator cuff tendon repair. *Journal of Shoulder and Elbow Surgery*, 16, 191S. <https://doi.org/10.1007/s11999-007-0112-4-633S>.
- Rücker, M., Laschke, M. W., Junker, D., Carvalho, C., Schramm, A., Mülhaupt, R., ... Menger, M. D. (2006). Angiogenic and inflammatory response to biodegradable scaffolds in dorsal skinfold chambers of mice. *Biomaterials Elsevier*, 27(29), 5027–5038. <https://doi.org/10.1016/J.BIOMATERIALS.2006.05.033>
- Schumann, P., von See, C., Kampmann, A., Lindhorst, D., Tavassol, F., Kokemüller, H., ... Rücker, M. (2011). Comparably accelerated vascularization by preincorporation of aortic fragments and mesenchymal stem cells in implanted tissue engineering constructs. *Journal of Biomedical Materials Research Part A. Wiley Subscription Services, Inc., A Wiley Company*, 97A(4), 383–394. <https://doi.org/10.1002/jbm.a.33069>
- Seyednejad, H., Gawlitta, D., Kuiper, R. V., de Bruin, A., van Nostrum, C. F., Vermonden, T., ... Hennink, W. E. (2012). In vivo biocompatibility and biodegradation of 3D-printed porous scaffolds based on a hydroxyl-functionalized poly(ϵ -caprolactone). *Biomaterials*, 33(17), 4309–4318. <https://doi.org/10.1016/j.biomaterials.2012.03.002>
- Singh, S., Wu, B. M., & Dunn, J. C. Y. (2012). Delivery of VEGF using collagen-coated polycaprolactone scaffolds stimulates angiogenesis. *Journal of Biomedical Materials Research. Part A*, 100(3), 720–727. <https://doi.org/10.1002/jbm.a.34010>
- Sinikovic, B., Schumann, P., Winkler, M., Kuestermeyer, J., Tavassol, F., von See, C., ... Rücker, M. (2011). Calvaria bone chamber—A new model for intravital assessment of osseous angiogenesis. *Journal of Biomedical Materials Research Part A. Wiley-Blackwell*, 99A(2), 151–157. <https://doi.org/10.1002/jbm.a.32955>
- Tallawi, M., Rosellini, E., Barbani, N., Cascone, M. G., Rai, R., Saint-Pierre, G., & Boccaccini, A. R. (2015). Strategies for the chemical and biological functionalization of scaffolds for cardiac tissue engineering: A review. *Journal of the Royal Society Interface*, 12(108), 20150254. <https://doi.org/10.1098/rsif.2015.0254>
- Tavassol, F., Kampmann, A., Schumann, P., Lindhorst, D., Kokemüller, H., Essig, H., ... Gellrich, N. C. (2011). A novel approach for studying microcirculation in bone defects by intravital fluorescence microscopy. *Tissue Engineering Part C: Methods*, 17, 1151–1159. <https://doi.org/10.1089/ten.tec.2011.0065>
- Venugopal, J., Ma, L. L., Yong, T., & Ramakrishna, S. (2005). In vitro study of smooth muscle cells on polycaprolactone and collagen nanofibrous matrices. *Cell Biology International*, 29, 861–867. <https://doi.org/10.1016/j.cellbi.2005.03.026>
- Walthers, C. M., Nazemi, A. K., Patel, S. L., Wu, B. M., & Dunn, J. C. (2014). The effect of scaffold macroporosity on angiogenesis and cell survival in tissue-engineered smooth muscle. *Biomaterials*, 35(19), 5129–5137. <https://doi.org/10.1016/j.biomaterials.2014.03.025>
- Wang, Z., Cui, Y., Wang, J., Yang, X., Wu, Y., Wang, K., ... Zhu, Y. (2014). The effect of thick fibers and large pores of electrospun poly(ϵ -caprolactone) vascular grafts on macrophage polarization and arterial regeneration. *Biomaterials*, 35(22), 5700–5710. <https://doi.org/10.1016/j.biomaterials.2014.03.078>
- Willbold, E., & Witte, F. (2010). Histology and research at the hard tissue-implant interface using Technovit 9100 New embedding technique. *Acta Biomaterialia Elsevier*, 6(11), 4447–4455. <https://doi.org/10.1016/J.ACTBIO.2010.06.022>
- Zelzer, E., Blitz, E., Killian, M. L., & Thomopoulos, S. (2014). Tendon-to-bone attachment: From development to maturity. *Birth Defects Research. Part C, Embryo Today: Reviews. NIH Public Access*, 102(1), 101–112. <https://doi.org/10.1002/bdrc.21056>
- Zimmerer, R. M., Ludwig, N., Kampmann, A., Bittermann, G., Spalthoff, S., Jungheim, M., ... Tavassol, F. (2017). CD24+ tumor-initiating cells from oral squamous cell carcinoma induce initial angiogenesis in vivo. *Microvascular Research Academic Press*, 112, 101–108. <https://doi.org/10.1016/J.MVR.2017.03.006>

SUPPORTING INFORMATION

Additional supporting information may be found online in the Supporting Information section at the end of the article.

Figure S1. Representative van Gieson stainings demonstrating foreign body giant cells (FBGC) in the control group (A), PCL-group (B) and CS-g-PCL group (C). Arrows denote FBGC. For semiquantitative analysis (D) ten excerpts were assessed in three histological cuts each for each implant.

How to cite this article: Gniesmer S, Brehm R, Hoffmann A, et al. In vivo analysis of vascularization and biocompatibility of electrospun polycaprolactone fibre mats in the rat femur chamber. *J Tissue Eng Regen Med*. 2019;13:1190–1202. <https://doi.org/10.1002/term.2868>